

Supplementary Information

Reaction of a sterically encumbered iron(I) aryl/arene with organoazides: formation of an iron(V) imide.[†]

Chengbao Ni, James C. Fettinger, Gary J. Long, Marcin Brynda and Philip P. Power

Magnetic Studies and 1 and 2

Experimental

The samples used for magnetic measurements were sealed under vacuum in 3 mm diameter quartz tubing. The sample magnetization was measured using a Quantum Design MPMSXL7 superconducting quantum interference magnetometer. For each measurement the sample was zero-field cooled to either 2 or 6 K and the moment was measured upon warming to 320 K in an applied field of 0.001 T. Additional time was allowed between each measurement at the lower temperatures to ensure thermal equilibrium between the sealed sample and the temperature sensor. Diamagnetic corrections of -0.000672 , -0.000591 , and -0.000455 emu/mol Fe, obtained from tables of Pascal's constants, have been applied to the measured susceptibility of **1-3**, respectively.

Results and Discussion

Magnetic Properties. The magnetic properties of **1** have been measured from 6 to 320 K in a 0.001 T applied field. The resulting effective magnetic moment, μ_{eff} , and the inverse molar magnetic susceptibility, $1/\chi_M$, are shown in Figure A. In **1** $1/\chi_M$ is linear from 6 to 320 K and yields a Curie constant, C , of 3.496 emu K/mol Fe, a Weiss temperature, θ , of -5 K, and a corresponding μ_{eff} of $5.29 \mu_B$, values that are fully consistent with the structure of **1** which contains two very well separated, virtually paramagnetic, high-spin, iron(II) ions.

A fit^{A,B} of either the observed μ_{eff} , see Figure A, or of $\chi_M T$, of **1** from 30 to 320 K yields $g = 2.167(2)$ and $J = -1.11 \text{ cm}^{-1}$, a fit that indicates the presence of weak, but not unexpected, intramolecular or intermolecular exchange coupling between the iron(II) ions. Below ca. 30 K the moment is somewhat higher than predicted on the basis of the exchange coupling fits and may indicate the presence of some single-ion zero-field splitting. [I have tried fits with D, but so far they fail. I will continue trying to do fits below 30 K.]

The magnetic properties of **2** have been measured from 2 to 320 K in a 0.001 T applied field; the resulting μ_{eff} , which decreases almost linearly from $2.74 \mu_B$ at 8 K to $2.43 \mu_B$ at 320 K, and $1/\chi_M$ are shown in Figure B. The plot of $1/\chi_M$ is not strictly linear but does correspond to the expected paramagnetic nature of **2**. Because of the curvature found in $1/\chi_M$, linear two least squares fits have been obtained. Between 2 and 100 K the fit yields a C of 0.914 emu K/mol Fe, a θ of 0.32 K, and a corresponding μ_{eff} of $2.70 \mu_B$. Between 200 and 300 K the fit yields a C of

0.632 emu K/mol Fe, a θ of 49 K, and a corresponding μ_{eff} of 2.25 μ_B . These results are consistent with the approximately trigonal iron(V) coordination environment of **2** and an iron(V) $3d^3$ electronic configuration with two paired electrons and one unpaired electron; the corresponding ground state could thus be a 2A , 2B , or 2E state. The exact reason for the virtually linear decrease in μ_{eff} upon warming from 8 to 320 K is not obvious but is probably the result of a combination of spin-orbit coupling, a varying orbital contribution, and a second order Zeeman contribution to the magnetic susceptibility. The decrease in μ_{eff} below 8 K is, no doubt, the result of weak long-range intermolecular antiferromagnetic exchange.

References and Notes

- (A) Ginsberg, A. P. *Inorg. Chim. Acta* **1971**, *5*, 45-68.
- (B) For the details of the Hamiltonian used in the fits see: Sutton, A. D.; Ngyuen, T.; Fettinger, J. C.; Olmstead, M. M.; Long, G. J.; Power, P. P. *Inorg. Chem.* **2007**, *46*, 4809-4814.

Figure Captions

Figure A. The temperature dependence of μ_{eff} of **1**. The solid line corresponds to a molecular exchange fit with $g = 2.167(2)$ and $J = -1.11(3) \text{ cm}^{-1}$. Inset: The temperature dependence of $1/\chi_M$ and its linear fit with the Curie-Weiss law.

Figure B. The temperature dependence of μ_{eff} of **2**. Inset: The temperature dependence of $1/\chi_M$ and its higher and lower temperature linear fits with the Curie-Weiss law.

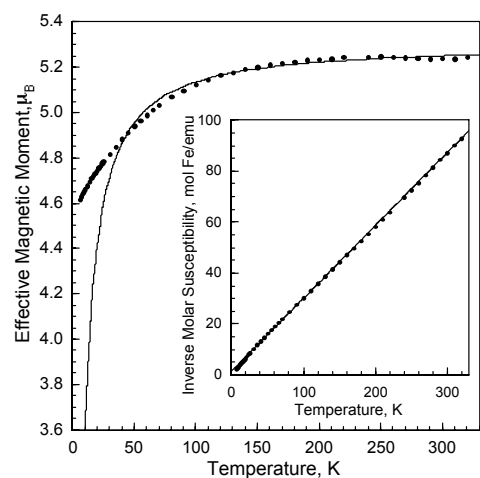


Figure A.

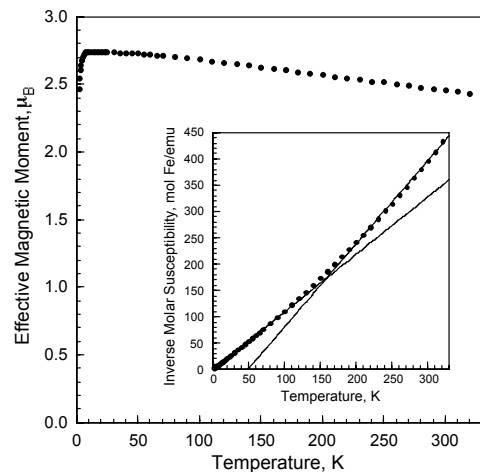


Figure B.

DFT calculations on model species M2

All the electronic structure calculations were performed with Gaussian 03 program [Ref R1] using several hybrid and pure functionals (see Table S1) combined with a double- ζ quality 6-31g* basis set or with Slater type orbitals using TZP basis set of triple quality and PBE0 functional, as implemented in ADF [Ref R2]. Optimization of the model compound **M2**, Ar*Fe(NBu^t)₂ (Ar* = (2,6-Ph)₂-C₆H₃) at various levels of theory yielded structural parameters reported in Table S1. The bond lengths, bond angles and the close-to-planarity structure of the C_{ipso}FeN(N) core are reproduced correctly (with the overall best agreement with experimental X-ray data for BLYP/6-31g(d) and B3LYP/6-31g(d) levels of theory) except for the N-Fe-N angle, which is clearly overestimated in all the optimized geometries. This is most likely due to steric constraints present in the Kohn-Sham crystal lattice due to the very large size of the terphenyl ligand.

The analysis for the Kohn-Sham [KS] orbitals shows that the unpaired electron is almost exclusively localized in the d_{xz} orbital of the iron, as visualized by the corresponding spin density plot (see Fig. S1) as well as the corresponding spin density from the Mulliken spin population analysis (Table S2). Only very slight spin polarization is observed on the nitrogen atoms. The HOMO can be described as a bonding π type orbital extending over the N-Fe-N core of the molecule, with essentially two p_z N orbitals in phase with the two lobes of the d_{xz} orbital of Fe, while the LUMO is essentially the same type of orbital with inversed phases for the nitrogen p_z orbitals.

Additional calculations performed on the fully symmetrized model species with reduced ligand size (PhFe(NMe)₂) where the orientation of the phenyl ring was set either coplanar, perpendicular or at 45° relative to the NFeNC_{ipso} plane (53° in the X-ray structure of the title compound), did not show any significant differences in the MO picture relative to this orientation, except for a very slight changes in the order of the molecular orbitals. Interestingly (and in accordance with the trend observed for the previously optimized **M2** structure), the lowest energy was obtained for the species where the phenyl ring is perpendicular to the NFeNC_{ipso} plane (relative energies for the perpendicular, 45° bent and planar forms are 0.0, +0.7 and +1.4 kcal mol⁻¹ respectively.). This probably explains the “intermediate” 53° Ph-NFeN angle obtained from the X-ray structure, that could be caused by the inability of the big terphenyl ligand to adopt a more perpendicular structure due to the steric constraints.

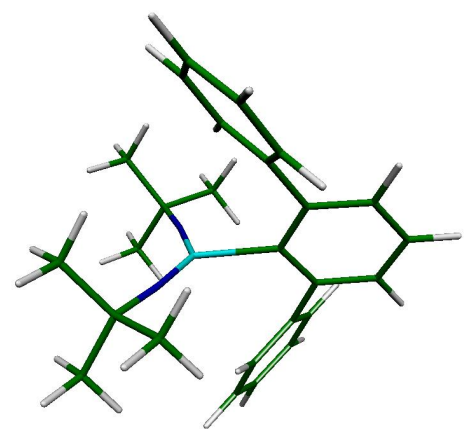


Figure S1. Geometry of the **M2** model species $\text{Ar}^*\text{Fe}(\text{NBu}^t)_2$ ($\text{Ar}^* = (2,6\text{-Ph})_2\text{-C}_6\text{H}_3$) optimized at BLYP/6-31g(d) level of theory.

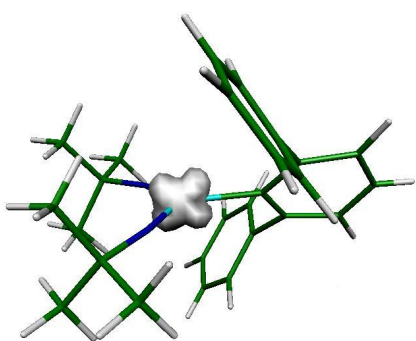


Figure S2. Plot of the spin density for the **M2** Kohn-Sham $\text{Ar}^*\text{Fe}(\text{NBu}^t)_2$ ($\text{Ar}^* = (2,6\text{-Ph})_2\text{-C}_6\text{H}_3$) species.

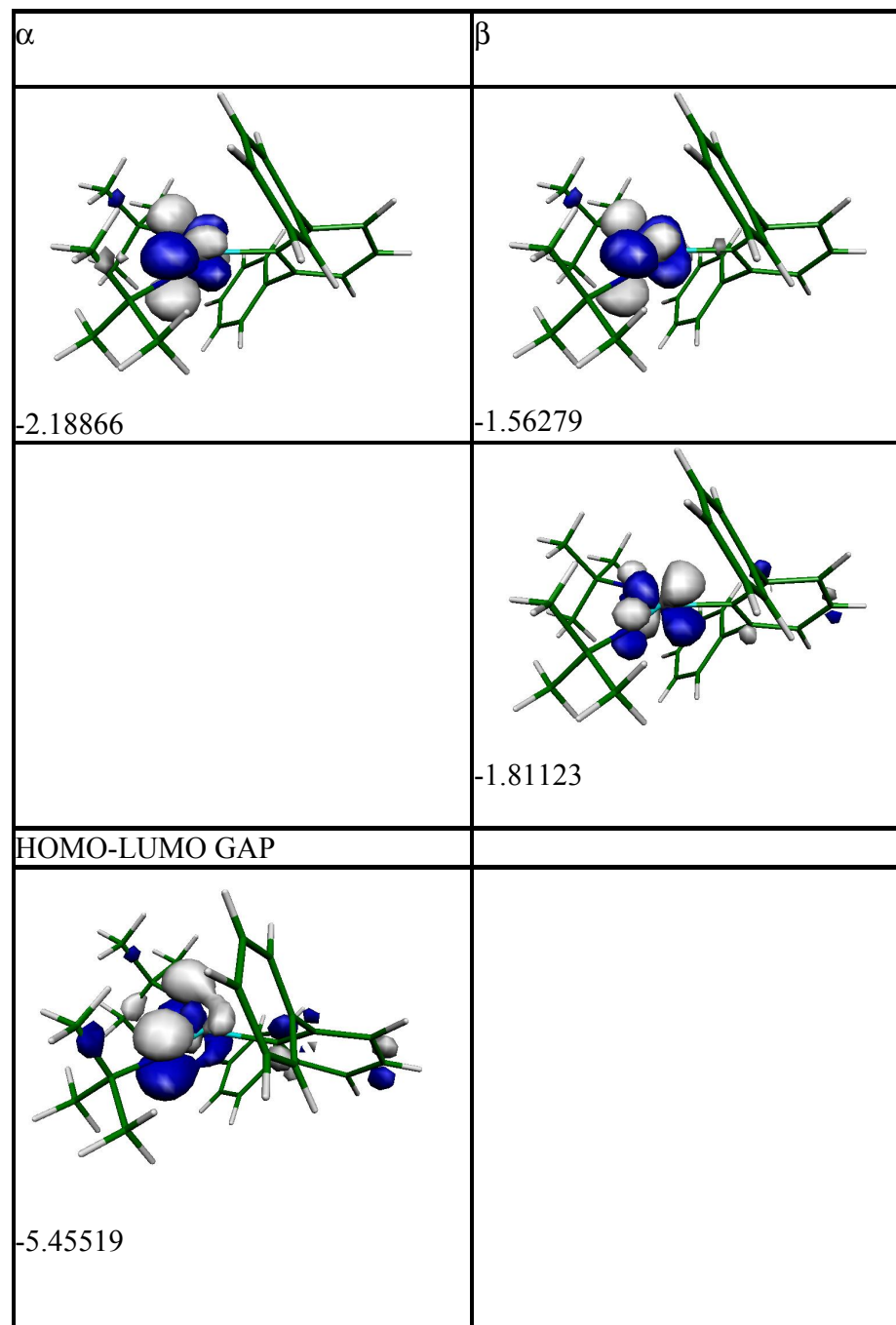
Theoretical level	$C_{ipso}Fe$	$Fe-N(1)/N(2)$	$C_{ipso}FeN(1)/N(2)$	$N(1)FeN(2)$	Planarity ¹	$CC_{ipso}FeN^2$
Experimental	2.013	1.619 (1.642)	118.6 (119.5)	121.9	359.8	51.7
B3LYP ^a /6-31g(d)	1.974	1.614 (1.614)	108.2 (108.5)	141.4	358.1	66.3
SVWN ^b /6-31g(d)	1.893	1.596 (1.597)	106.0 (106.8)	138.4	351.2	51.3
PBE0 ^c /6-31g(d)	1.948	1.615 (1.616)	109.8 (109.9)	136.4	356.1	59.7
BLYP ^d /6-31g(d)	1.973	1.624 (1.625)	111.5 (112.1)	133.4	357.0	63.5
HCTH ^e /6-31g(d)	1.959	1.606 (1.608)	111.1 (112.2)	133.4	356.7	63.7
PBE0 ^c /TZP (STO)	1.968	1.621 (1.622)	108.3 (108.7)	140.4	357.4	60.4

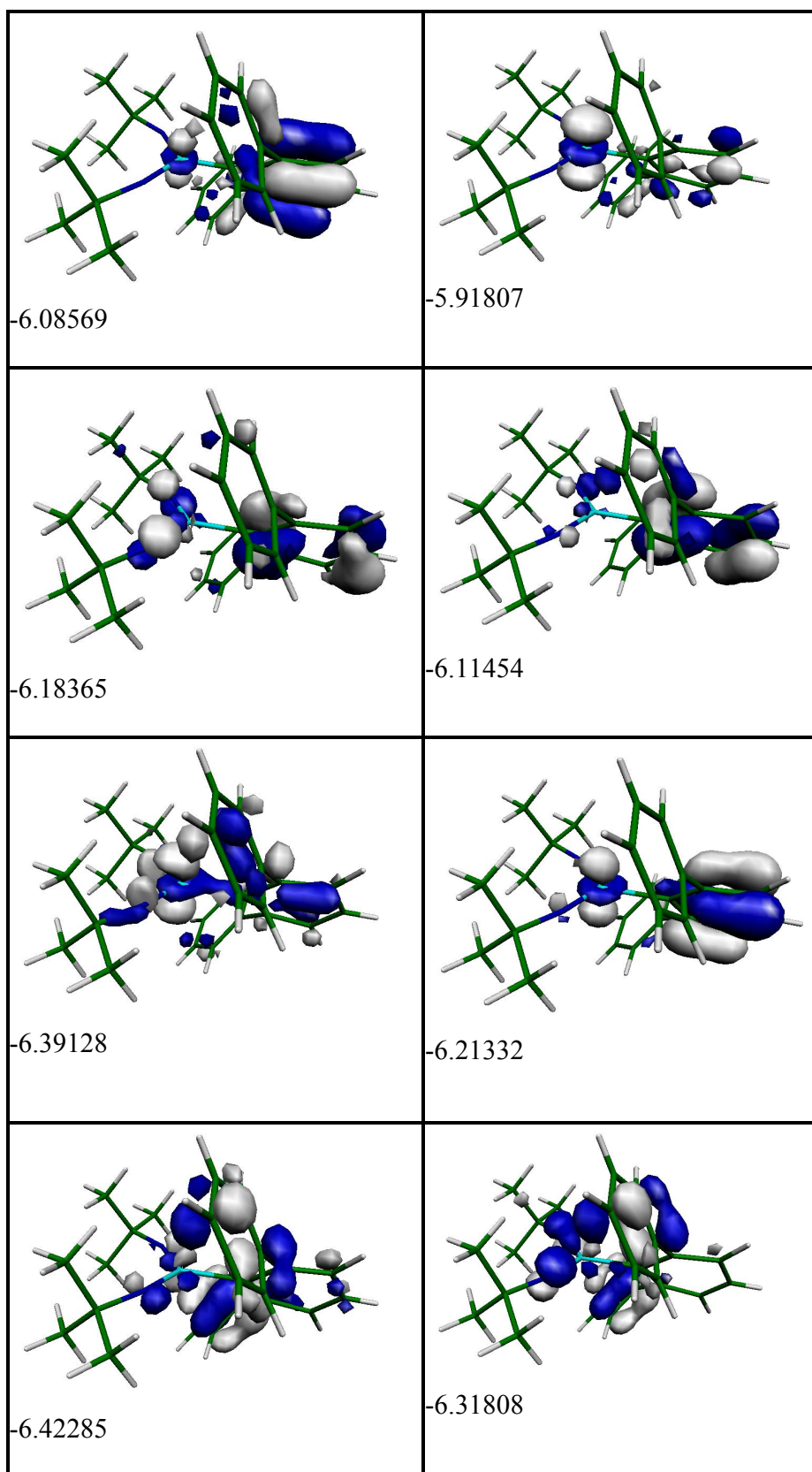
Table S1. Important geometrical parameters of the optimized **M2** model species. ¹Calculated as $\Sigma \alpha(C_{ipso}FeN(1) + C_{ipso}FeN(2) + N(1)FeN(2))$. ²By convention, the smallest angle is reported. ^a**B3LYP** is Becke three parameter hybrid functional with the correlation functional of Lee, Yang, and Parr using local and non-local terms. LYP provides the non-local correlation, while the local correlation is provided by VWN Vosko, Wilk, and Nusair 1980 correlation functional functional. ^b**SVWN** of a Local Spin Density Approximation (LSDA) type uses the Slater exchange and the **VWN** correlation functional of Vosko, Wilk, and Nusair. ^c**PBE0** is a hybrid functional using the exchange term of Perdew, Burke and Ernzerhof and a gradient-corrected correlation functional of the same authors. ^d**BLYP** is a pure gradient corrected LSDA method functional using exchange correction of Becke and the correlation function of Lee, Yang and Parr. ^e**HCTH** is Handy's family functional (HCTH/407) including gradient-corrected correlation.

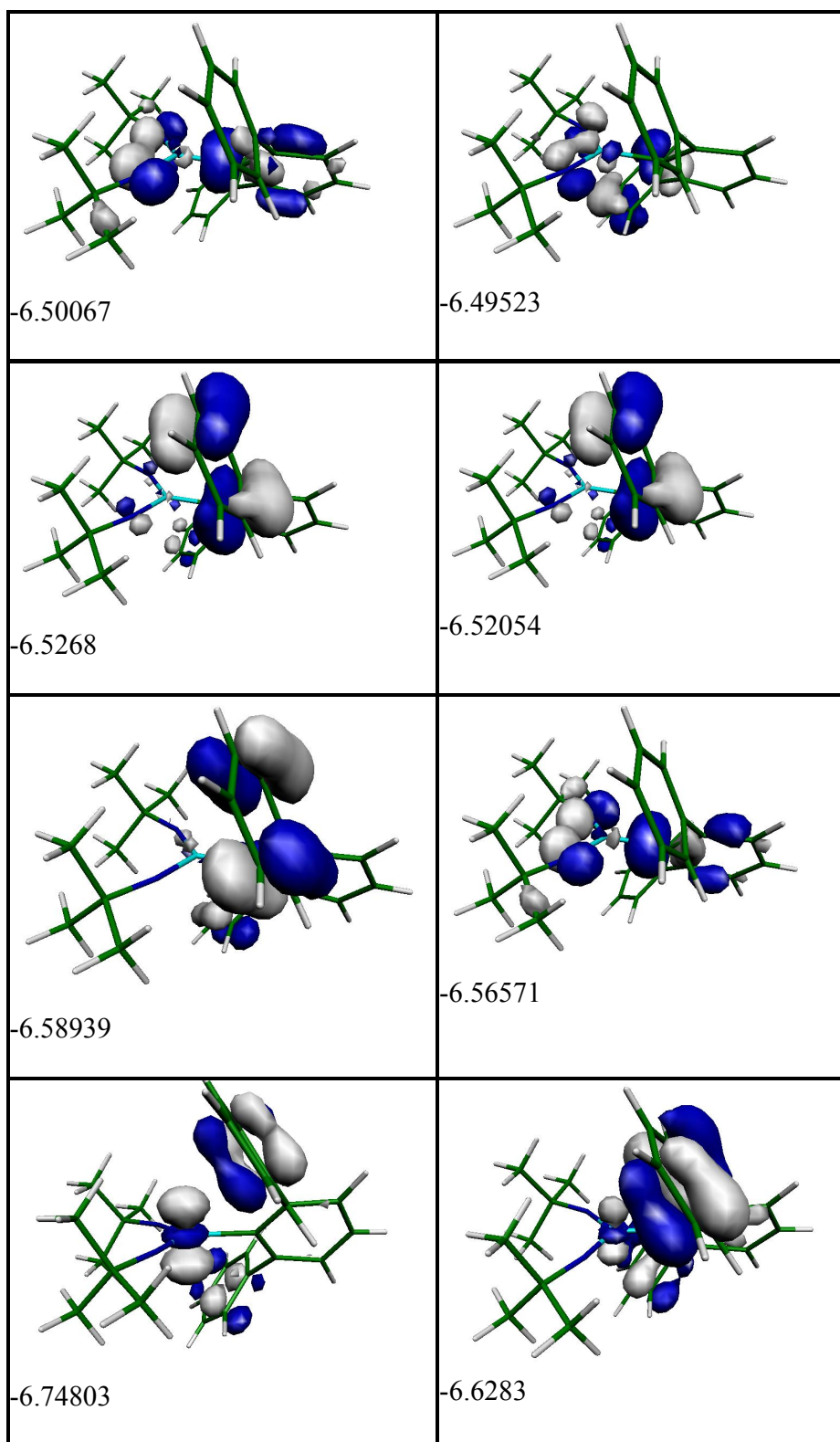
Atom	C_{ipso}	Fe	$N(1)$	$N(2)$	$C(CH_3)_3$
Spin density	-0.049	1.050	-0.018	-0.025	0.017

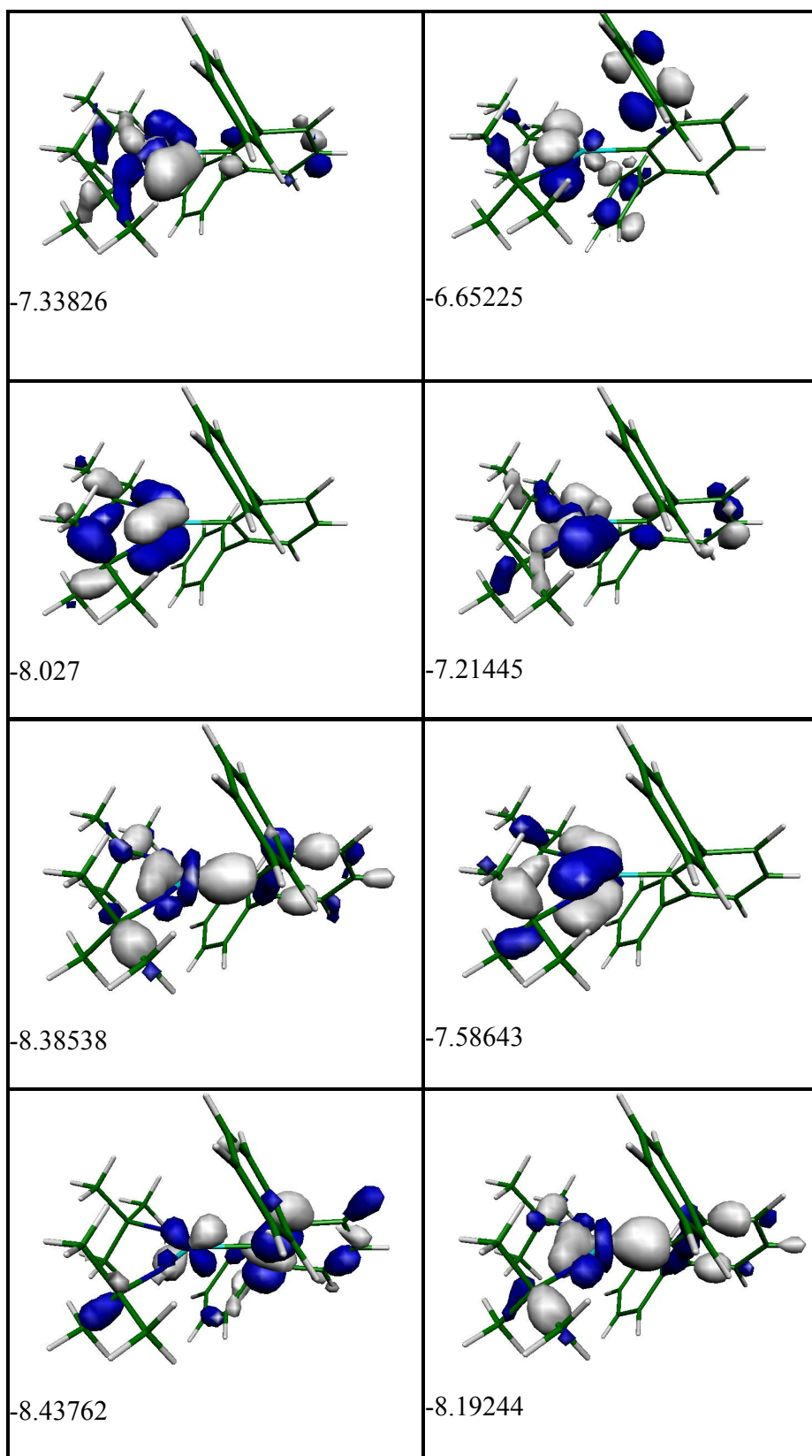
Table S2. Mulliken spin densities for selected atoms in the optimized geometry of **M2** obtained at PBE0/TZP level of theory.

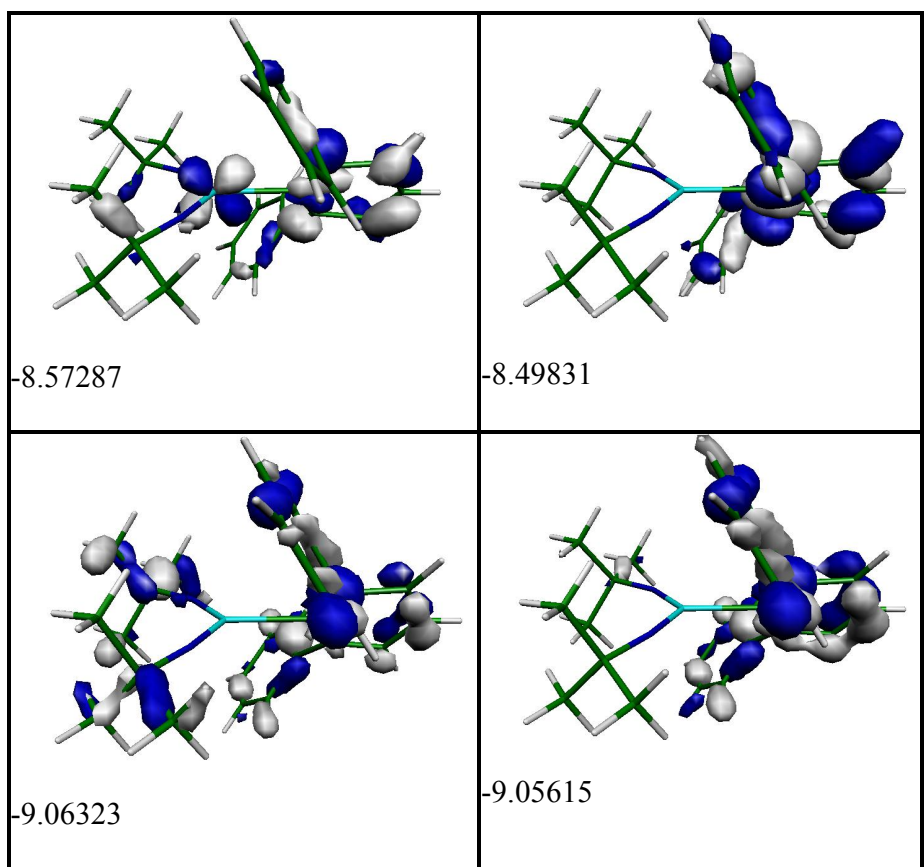
Relevant KS-MO's for the **M2** model species obtained at B3LYP/6-31g(d) level of theory.
Orbital energies in [eV].



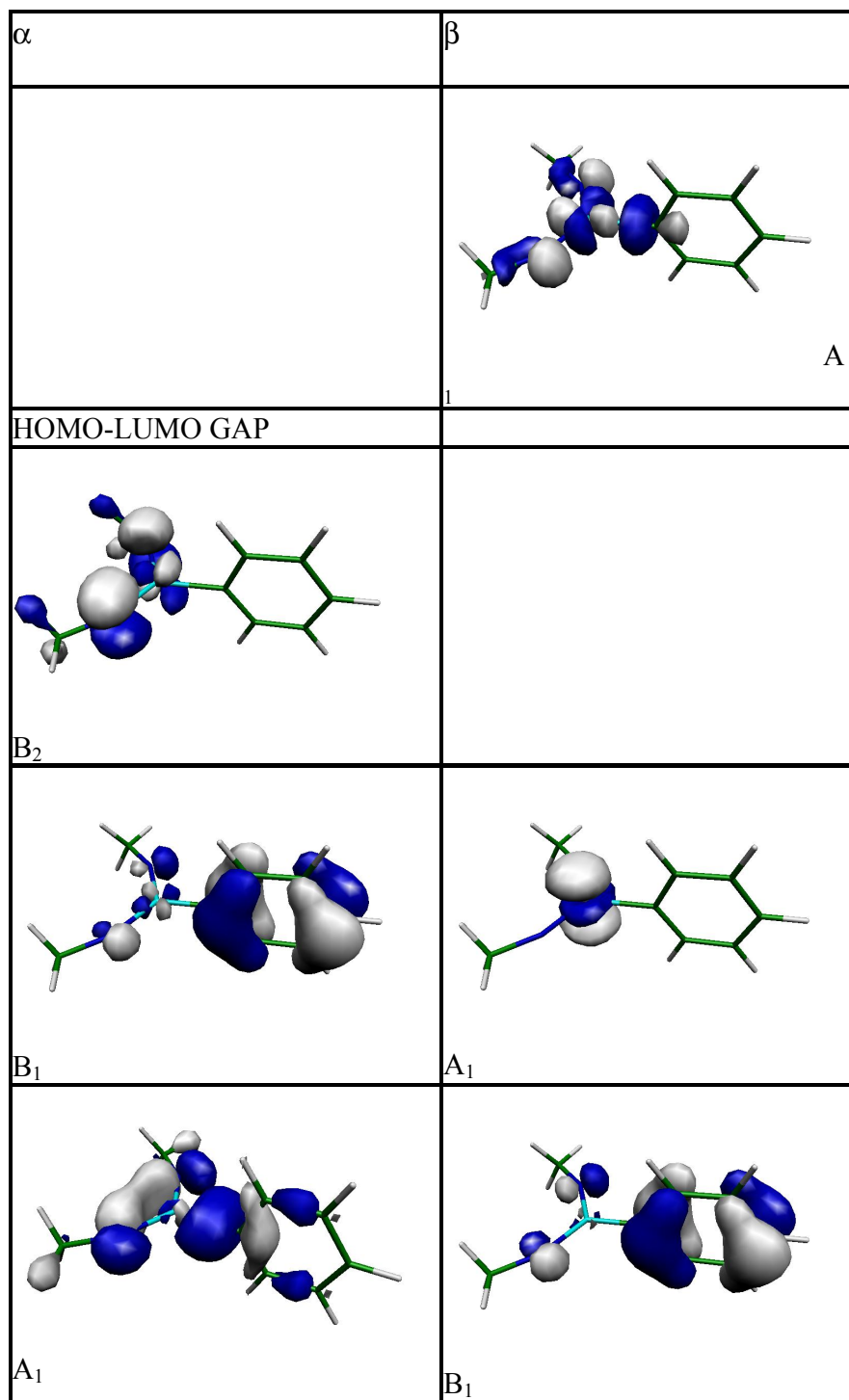


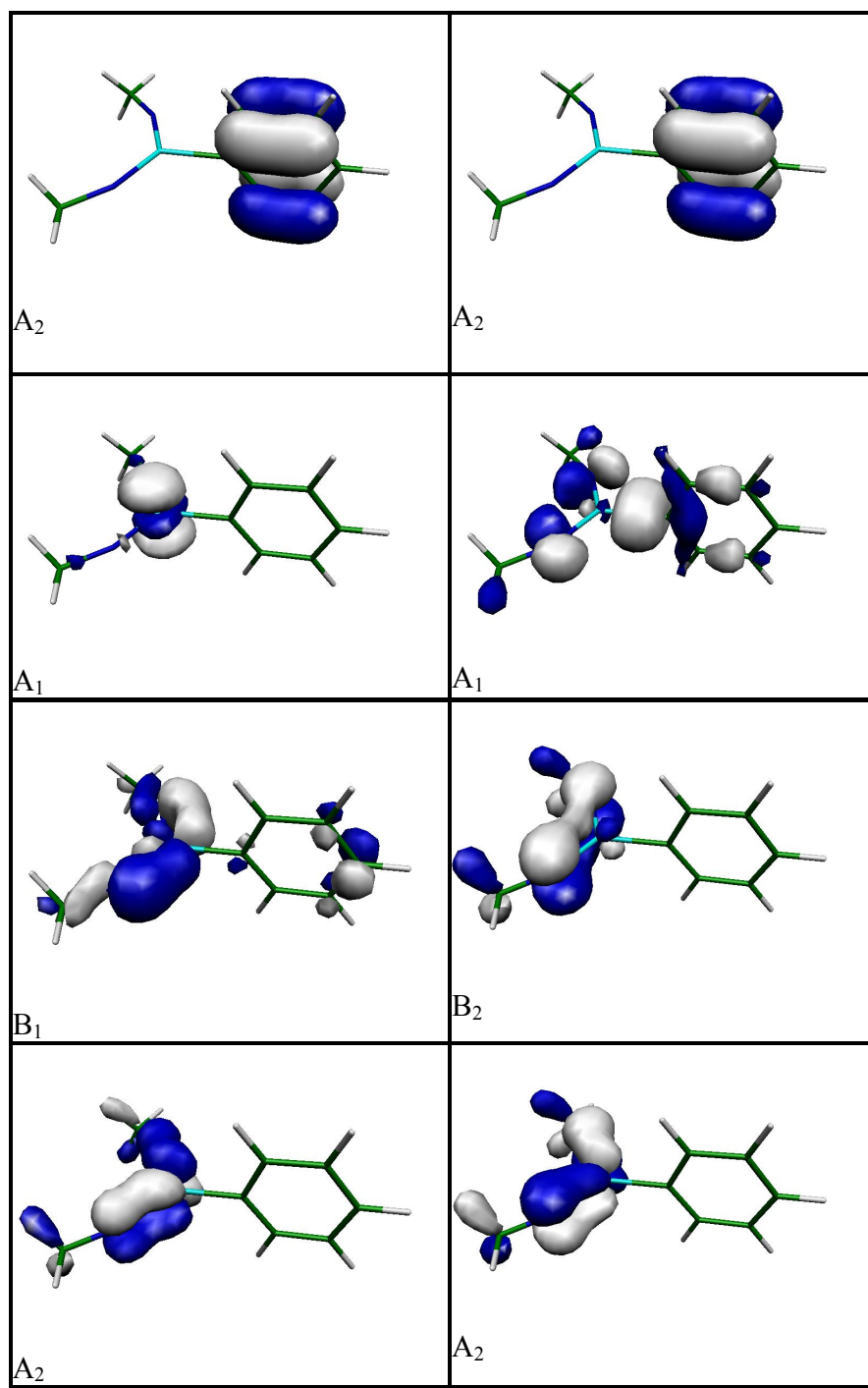


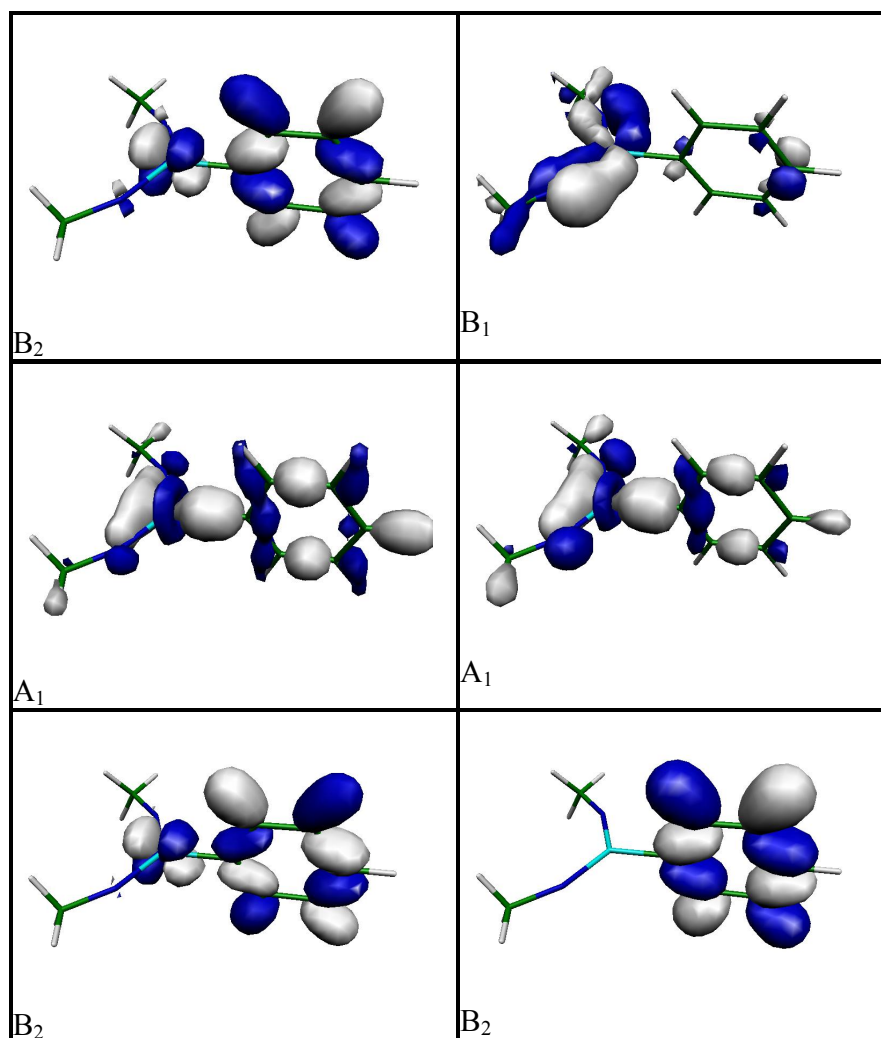




Relevant KS orbitals for the PhFe(NMe₂)₂ model species in perpendicular conformation (phenyl ring perpendicular to the NFeN fragment) with the corresponding symmetry labels.
Computed electronic state = ²B₂.







References

- (R1) Frisch, M. J.; Trucks, G. W.; Schlegel, H. B.; Scuseria, G. E.; Robb, M. A.; Cheeseman, J. R.; Montgomery, J. A., Jr.; Vreven, T.; Kudin, K.N.; Burant, J. C.; Millam, J. M.; Iyengar, S. S.; Tomasi, J.; Barone, V.; Mennucci, B.; Cossi, M.; Scalmani, G.; Rega, N.; Petersson, G. A.; Nakatsuji, H.; Hada, M.; Ehara, M.; Toyota, K.; Fukuda, R.; Hasegawa, J.; Ishida, M.; Nakajima, T.; Honda, Y.; Kitao, O.; Nakai, H.; Klene, M.; Li,X.; Knox, J. E.; Hratchian, H. P.; Cross, J. B.; Adamo, C.; Jaramillo, J.;Gomperts, R.; Stratmann, R. E.; Yazyev, O.; Austin, A. J.; Cammi, R.; Pomelli, C.; Ochterski, J. W.; Ayala, P. Y.;

Morokuma, K.; Voth, G. A.; Salvador, P.; Dannenberg, J. J.; Zakrzewski, V. G.; Dapprich, S.; Daniels, A. D.; Strain, M. C.; Farkas, O.; Malick, D. K.; Rabuck, A. D.; Raghavachari, K.; Foresman, J. B.; Ortiz, J. V.; Cui, Q.; Baboul, A. G.; Clifford, S.; Cioslowski, J.; Stefanov, B. B.; Liu, G.; Liashenko, A.; Piskorz, P.; Komaromi, I.; Martin, R. L.; Fox, D. J.; Keith, T.; Al-Laham, M. A.; Peng, C. Y.; Nanayakkara, A.; Challacombe, M.; Gill, P. M. W.; Johnson, B.; Chen, W.; Wong, M. W.; Gonzalez, C.; Pople, J. A. *Gaussian 03, Revision D.1*; Gaussian, Inc.: Pittsburgh, PA, 2003.

(R2) ADF *ADF2006.01, SCM, Theoretical Chemistry, Vrije Universiteit, Amsterdam, The Netherlands*, <http://www.scm.com..>